Supplementary information

Smaller rare-earth cation and mixed valent Mn incorporation as a dual strategy to enhance ferrimagnetic ordering temperatures in A-site ordered quadruple perovskites, $LnCu_3Mn_{1+x}Ti_{3-x}O_{12}$ (Ln = La, Nd; x = 0, 0.3)

Lalit Kumar,[a, b] Sujan Sen[a] and Tapas Kumar Mandal*[, a, c]

[a]Department of Chemistry, Indian Institute of Technology Roorkee, Roorkee – 247667, India

[b]Department of Applied Science and Humanities, Invertis University, Bareilly – 243123, India

[c]Center for Nanotechnology, Indian Institute of Technology Roorkee, Roorkee – 247667, India.

Corresponding author:

*E-mail: tapas.mandal@cy.iitr.ac.in

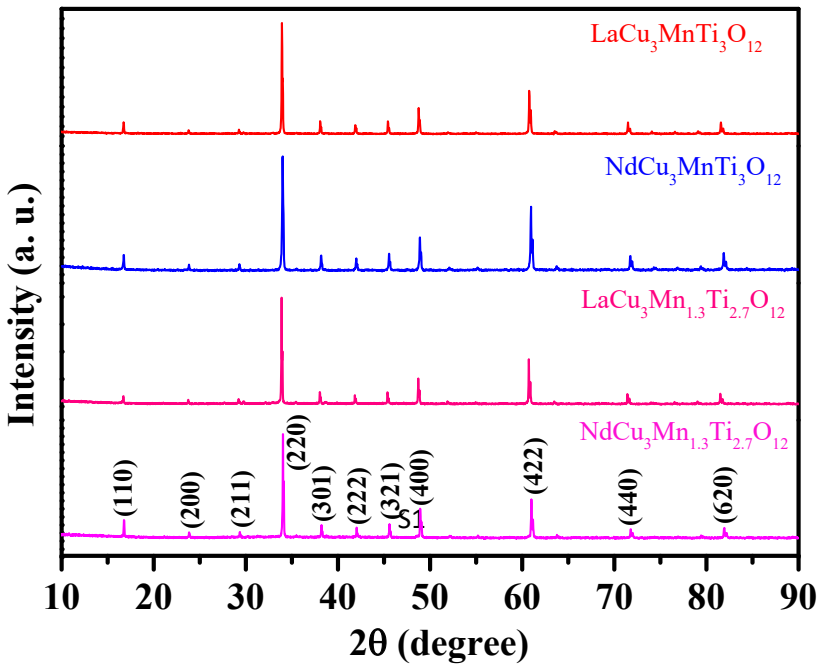

Fig. S1 P-XRD patterns of (a) $LaCu_3MnTi_3O_{12}$, (b) $NdCu_3MnTi_3O_{12}$, (c) $LaCu_3Mn_{1.3}Ti_{2.7}O_{12}$, and (d) $NdCu_3Mn_{1.3}Ti_{2.7}O_{12}$.

Table S1 Refined positional (x, y, z), thermal (B), occupancy parameters and reliability factors for $LnCu_3Mn_{1+x}Ti_{3-x}O_{12}$ (Ln = La, Nd; x = 0, 0.3)

Atom	Site	Position	$LaCu_3MnTi_3O_{12}$	$NdCu_3MnTi_3O_{12}$	$LaCu_3Mn_{1.3}Ti_{2.7}O_{12}$	$NdCu_3Mn_{1.3}Ti_{2.7}O_{12}$

a (Å)			7.4663(6)	7.4526(8)	7.4515(6)	7.4363(5)
O	24g	*x*	0.3042(1)	0.3014(5)	0.3176(1)	0.3020(9)
		y	0.1819(1)	0.1799(4)	0.1910(4)	0.1801(2)
Occ $(Mn/Ti)_{8c}$			0.25/0.75	0.25/0.75	0.325/0.675	0.325/0.675
B(Å^2) $(A)_{2a}$			0.32(4)	0.42(5)	0.65(1)	0.78(1)
B(Å^2) $(Cu)_{6b}$			0.18(2)	0.32(4)	0.48(4)	0.67(6)
B(Å^2) $(Mn/Ti)_{8c}$			0.25(3)	0.51(3)	0.36(4)	0.75(5)
B(Å^2) $(O)_{24g}$			0.81(6)	0.78(8)	0.98(8)	0.87(9)
R_p (%)			3.62	4.21	6.14	4.15
R_{wp} (%)			5.12	5.73	7.20	6.18
R_{Bragg} (%)			2.76	4.08	5.64	4.57
R_F (%)			2.11	2.29	4.61	2.71
χ^2			2.79	2.27	4.57	3.10

Atomic positions: La/Nd 2a (0, 0, 0), Cu 6b (0, 0.5, 0.5), Mn/Ti 8c (0.25, 0.25, 0.25), O 24g (*x*, *y*, 0). The occupancy of rest La/Nd, Cu and O are 1. A = La or Nd.

Lengths (Å);	**$LaCu_3MnTi_3O_{12}$**	**$NdCu_3MnTi_3O_{12}$**	**$LaCu_3Mn_{1.3}Ti_{2.7}O_{12}$**	**$NdCu_3Mn_{1.3}Ti_{2.7}O_{12}$**
Angles (°);				

BVS				
*A – O (× 12)	2.633(7)	2.603(7)	2.631(4)	2.602(9)
Cu – O (× 4)	1.985(7)	1.987(8)	1.983(4)	1.980(8)
Mn/Ti – O (× 6)	1.966(3)	1.963(3)	1.965(3)	1.958(5)
∠Mn/Ti – O – Mn/Ti	141.6(3)	141.7(8)	140.5(8)	141.5(8)
∠Mn/Ti – O – Cu	108.9(4)	108.8(4)	109.7(4)	108.7(4)
*∠A – O – Cu	106.2(6)	107.0(7)	102.2(6)	106.6(6)
*∠A – O – Mn/Ti	87.5(4)	88.2(4)	84.1(4)	88.6(5)
BVS (A)*	3.28	3.12	3.26	3.31
BVS (Cu)	1.75	1.82	1.80	1.72
BVS (Mn/Ti)	3.84	3.86	3.70	3.96
*A = La or Nd				

Table S2 Bond lengths, bond angles and bond valence sums of $LnCu_3Mn_{1+x}Ti_{3-x}O_{12}$ (Ln = La, Nd; x = 0, 0.3)

Fig. S2 FE-SEM images of (a) $LaCu_3MnTi_3O_{12}$, (b) $NdCu_3MnTi_3O_{12}$, (c) $LaCu_3Mn_{1.3}Ti_{2.7}O_{12}$, and (d) $NdCu_3Mn_{1.3}Ti_{2.7}O_{12}$.

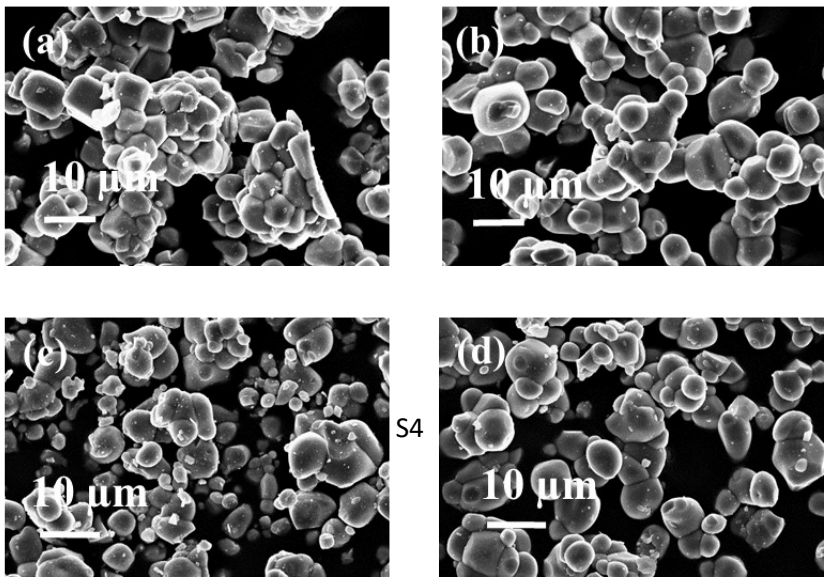

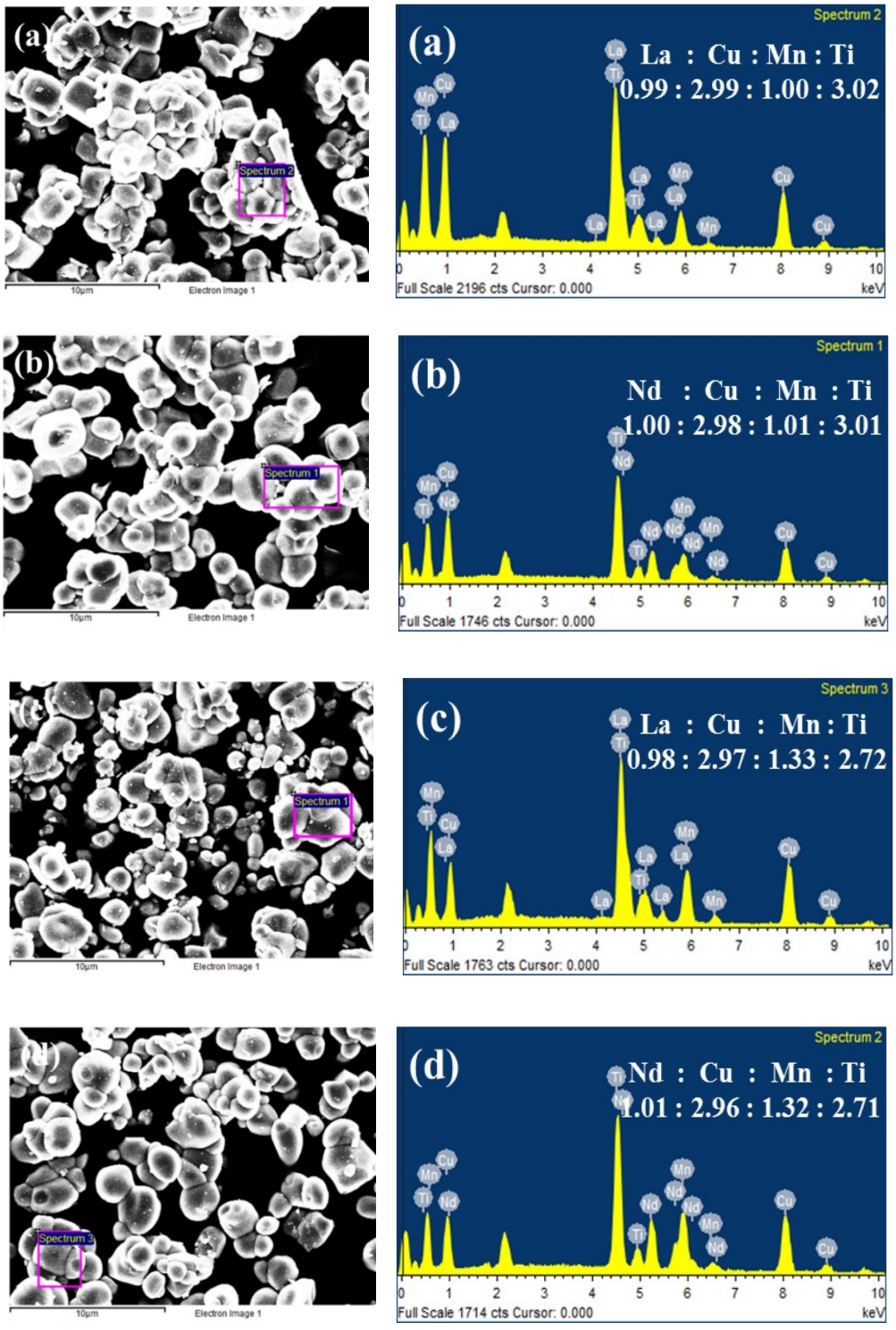

Fig. S3 EDS data of (a) $LaCu_3MnTi_3O_{12}$, (b) $NdCu_3MnTi_3O_{12}$, (c) $LaCu_3Mn_{1.3}Ti_{2.7}O_{12}$, and (d) $NdCu_3Mn_{1.3}Ti_{2.7}O_{12}$.

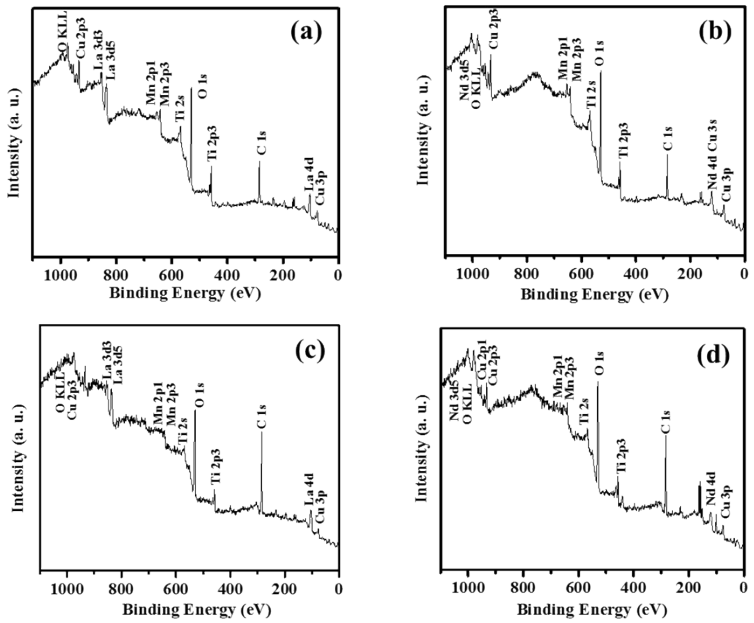

Fig. S4 Survey XPS spectra of (a) $LaCu_3MnTi_3O_{12}$, (b) $NdCu_3MnTi_3O_{12}$, (c) $LaCu_3Mn_{1.3}Ti_{2.7}O_{12}$, and (d) $NdCu_3Mn_{1.3}Ti_{2.7}O_{12}$.

Table S3 XPS binding energies of $LaCu_3MnTi_3O_{12}$, $NdCu_3MnTi_3O_{12}$, $LaCu_3Mn_{1.3}Ti_{2.7}O_{12}$, and $NdCu_3Mn_{1.3}Ti_{2.7}O_{12}$

Compounds	$LaCu_3MnTi_3O_{12}$	$NdCu_3MnTi_3O_{12}$	$LaCu_3Mn_{1.3}Ti_{2.7}O_{12}$	$NdCu_3Mn_{1.2}Ti_{2.7}O_{12}$	Ref.
Mn $2p_{3/2}$ (eV)	641.7	641.4	641.6 (Mn^{3+})	641.5 (Mn^{3+})	
			643.5(Mn^{4+})	643.7(Mn^{4+})	1
Mn $2p_{1/2}$ (eV)	653.2	653.3	652.7(Mn^{3+})	652.5(Mn^{3+})	
			654.2 (Mn^{4+})	654.8 (Mn^{4+})	1
Cu $2p_{3/2}$ (eV)	933.5	933.2	933.8	933.6	2
Cu $2p_{1/2}$ (eV)	953.7	953.4	953.7	953.6	2

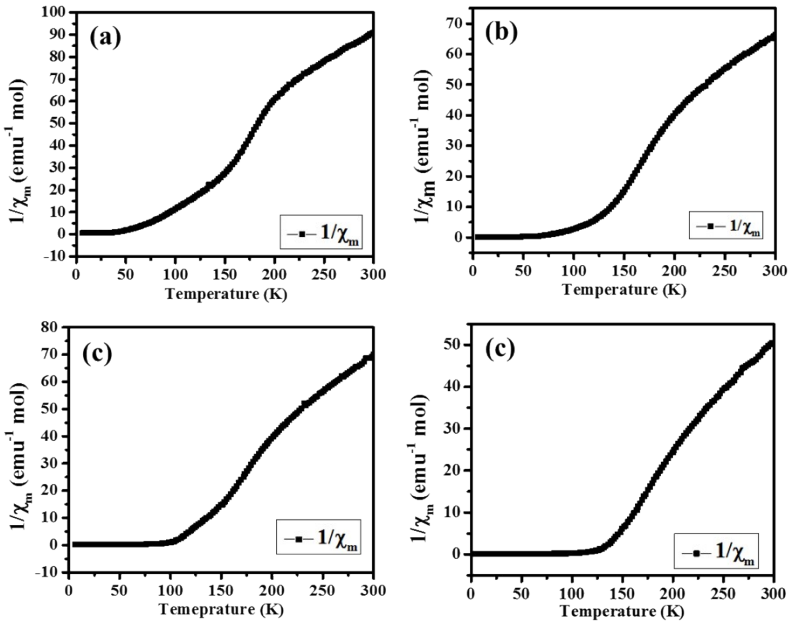

Fig. S5 Inverse magnetic susceptibility vs. temperature plots of (a) $LaCu_3MnTi_3O_{12}$, (b) $NdCu_3MnTi_3O_{12}$, (c) $LaCu_3Mn_{1.3}Ti_{2.7}O_{12}$, and (d) $NdCu_3Mn_{1.3}Ti_{2.7}O_{12}$.

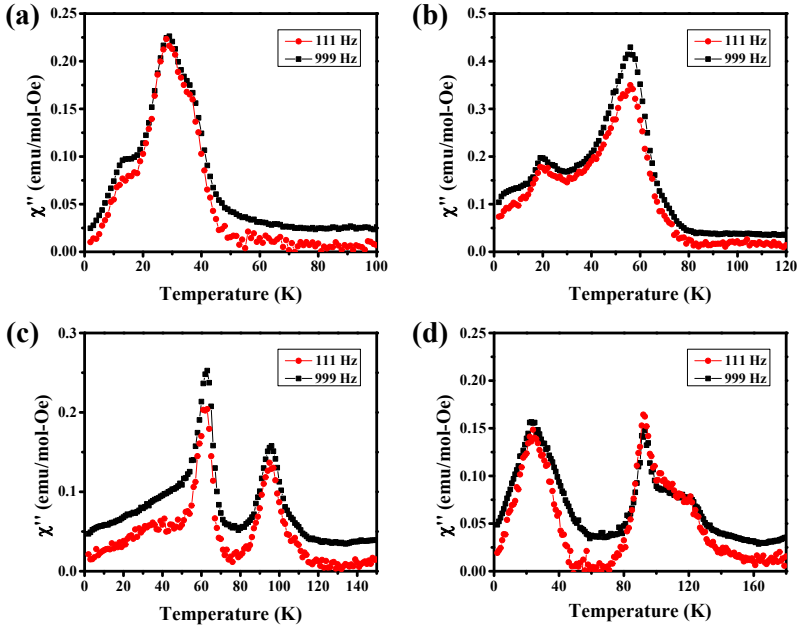

Fig. S6 χ´´ vs. T plots of (a) $LaCu_3MnTi_3O_{12}$, (b) $NdCu_3MnTi_3O_{12}$, (c) $LaCu_3Mn_{1.3}Ti_{2.7}O_{12}$, and (d) $NdCu_3Mn_{1.3}Ti_{2.7}O_{12}$

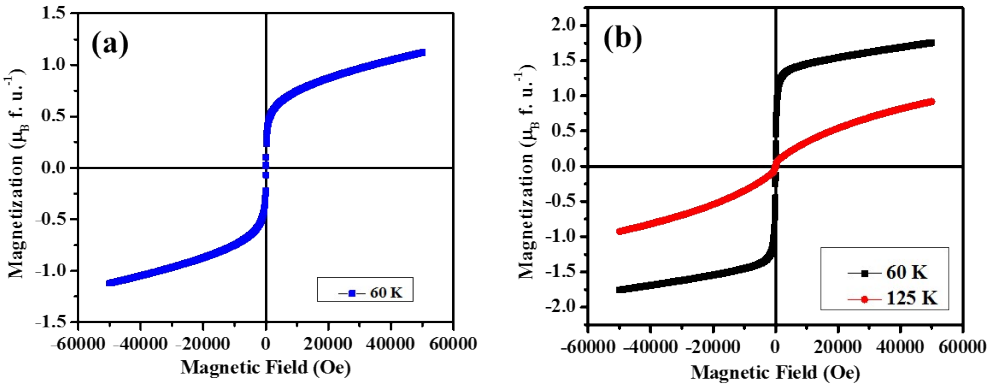

Fig. S7 Magnetization vs. magnetic field plots of (a) $NdCu_3MnTi_3O_{12}$ at 60 K, and (b) $NdCu_3Mn_{1.3}Ti_{2.7}O_{12}$ at 60 and 125 K.

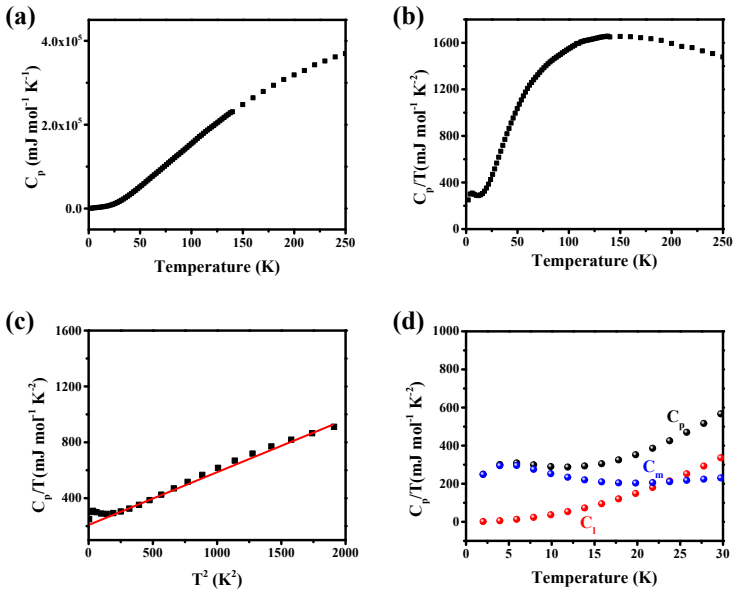

Fig. S8 Heat capacity data (a) C_p vs. T, (b) C_p/T vs. T, (c) C_p/T vs. T^2 and (d) lattice contribution (red) and magnetic contribution (blue) to total heat capacity (black) of $LaCu_3Mn_{1.3}Ti_{2.7}O_{12}$.

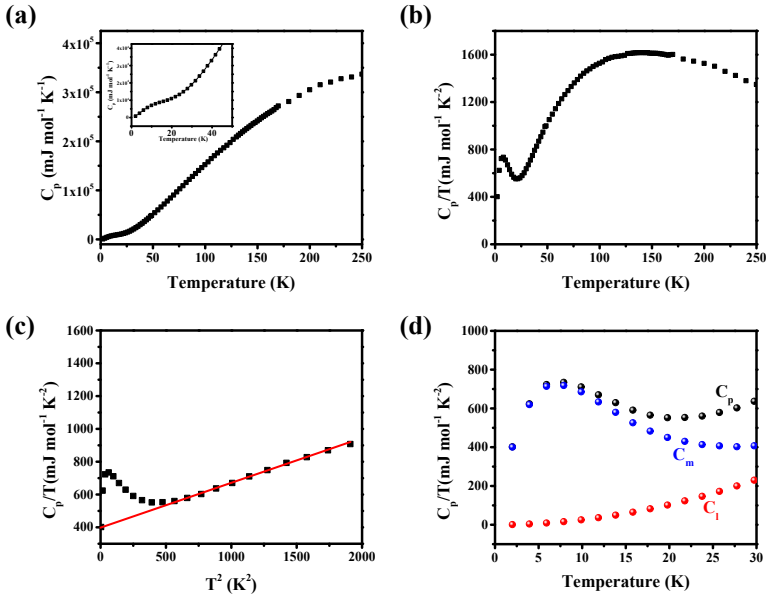

Fig. S9 Heat capacity data (a) C_p vs. T, (b) C_p/T vs. T, (c) C_p/T vs. T^2 and (d) lattice contribution (red) and magnetic contribution (blue) to total heat capacity (black) of $NdCu_3Mn_{1.3}Ti_{2.7}O_{12}$.

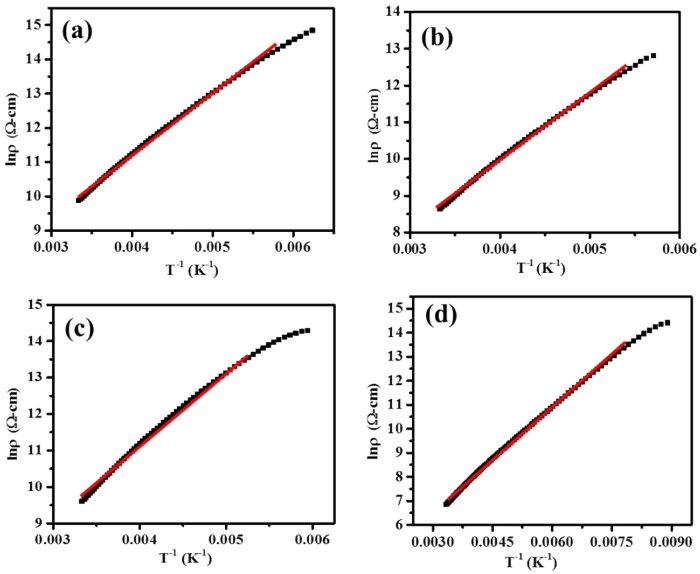

Fig. S10 $ln\rho$ vs. T^{-1} of (a) $LaCu_3MnTi_3O_{12}$, (b) $NdCu_3MnTi_3O_{12}$, (c) $LaCu_3Mn_{1.3}Ti_{2.7}O_{12}$, and (d) $NdCu_3Mn_{1.3}Ti_{2.7}O_{12}$.

References

1 M. C. Biesinger, L. W. M. Lau, A. R. Gerson, R. S. C. Smart, *Appl. Surf. Sci.*, 2010, **257**, 887.
2 M. Oku, K. Hirokawa, S. Ikeda, *J. Electron Spectrosc. Related Phenom*., 1975, **7**, 465.